Aerogel Cherenkov Counters of the KEDR Detector

I.V. Ovtin,[1,2] *A.Y. Barnyakov,*[1,2] *M.Y. Barnyakov,*[1,2] *V.S. Bobrovnikov,*[1,2] *A.R. Buzykaev,*[1,2] *A.F. Danilyuk,*[2,3], *A.A. Katcin,*[1,2] *S.A. Kononov,*[1,2] *E.A. Kravchenko,*[1,2] *I.A. Kuyanov,*[1,2] *A.P. Onuchin,*[1,2,4] *and V.A. Rodiakin*[1]
[1]Budker Institute of Nuclear Physics, Novosibirsk, Russia
[2]Novosibirsk State University, Novosibirsk, Russia
[3]Boreskov Institute of Catalysis, Novosibirsk, Russia
[4]Novosibirsk State Technical University, Novosibirsk, Russia

Abstract
The particle identification system of the KEDR detector is based on aerogel threshold Cherenkov counters called ASHIPH counters. The system consists of 160 counters arranged in two layers. An event reconstruction program for the ASHIPH system was developed. The position of each counter relative to the tracking system was determined using cosmic muons and Bhabha events. The geometric efficiency of the ASHIPH system was verified with Bhabha events. The efficiency of relativistic particle detection was measured with cosmic muons. A π/K separation of 4σ in the momentum range $0.95 - -1.45$ GeV/c was confirmed. A simulation program for the ASHIPH counters has been developed.

Keywords
Particle identification; ASHIPH; aerogel.

1 Introduction

The ASHIPH (Aerogel, SHifter, PHotomultiplier) method of Cherenkov light collection was suggested in 1992 [1–3]. Cherenkov light produced by traversing charged particles in the aerogel is transported by a wavelength shifter (WLS) placed in the middle of the counter to a photomultiplier (PMT). This method, compared with direct light collection, helped us to significantly decrease the PMT photocathode area and thus the cost of the system.

In 2014, the fully installed particle identification system of ASHIPH counters began operation in the KEDR experiment at the VEPP-4M e^+e^--collider. The system consists of 160 counters arranged in two layers (80 barrel counters and 80 endcap counters) and covers 96% of the total solid angle (Fig. 1). The counters are arranged in such a way that a particle travelling from the beam interaction point with a momentum larger than 0.6 GeV/c passes through at least two layers of counters. Constructions of the endcap and barrel counters are shown in Figs. 2 and 3, respectively. The total volume of the aerogel is 1000 litres. It has a refractive index $n = 1.05$. The system permits π/K separation for particles with momenta from 0.6 to 1.5 GeV/c [4]. A total of 160 microchannel plate PMTs with a multi-alkali photocathode with a diameter of 18 mm capable of working in a magnetic field of 2 T are used as the photon detectors.

2 Operation of the ASHIPH system in the KEDR experiment

2.1 High voltage supply

The high voltage (HV) source for microchannel plate PMTs consists of six HV converters H40N (EMCO: 4000 V, 3.75 mA, 15 W) in one standard CAMAC 4M module and was developed at BINP. Ten HV modules (PNPI, St. Petersburg) of 16-channel active HV dividers provide tuning of voltage for each counter from 2500 to 4000 V [5].

https://doi.org/10.23727/CERN-Proceedings-2017-001.187

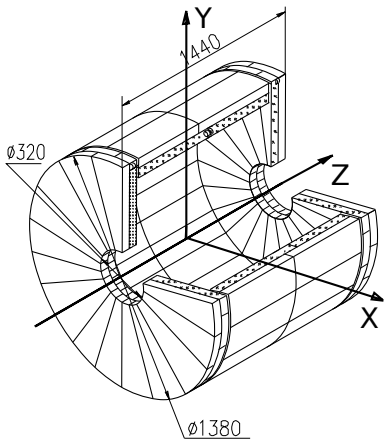

Fig. 1: Layout of the ASHIPH system of the KEDR detector.

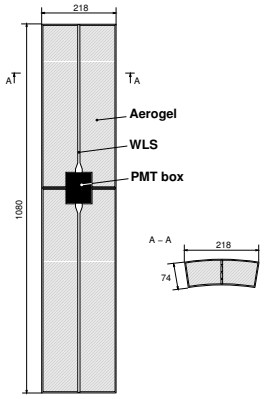

Fig. 2: Two barrel counters in a single housing.

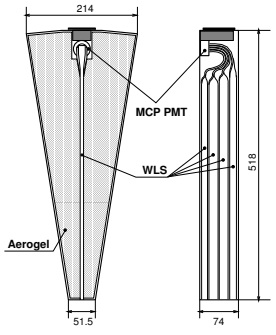

Fig. 3: Endcap counter.

2.2 Electronics

A charge from the photomultiplier anode is converted by the charge-sensitive preamplifier to the para-phase (bipolar) signal that is brought out of the detector. It is then supplied to inputs of digitizing boards via a long cable (40 m).

The data acquisition system of the KEDR detector is based on the KLUKVA electronic standard developed at BINP [6]. The counters are read out by 28 dedicated A6 electronics boards, which work in the pipeline mode. An A6 board has six channels. Basic elements of the circuit are a 10 bit flash analogue-to-digital converter (ADC) and a shift register. The ADC measures an instantaneous voltage value with a period of 55 ns. The shift register serves as data storage for the trigger-operation time. Five values of voltage are read out for each pulse. There is a discriminator in the circuit to monitor the dark count rates of the PMTs [5, 7].

2.3 Slow control system

The slow control system monitors the dark count rates of the PMTs and provides HV power control. In an emergency, each counter is switched off by an active HV divider individually. The gain stability and counter efficiency are monitored twice per week during calibration runs with LEDs and cosmic particles [5].

3 Event reconstruction and alignment of the ASHIPH system

The event reconstruction program of the ASHIPH system consists of two stages. In the first stage, the recorded pulse shape of five hit amplitudes is fitted to determine the amplitude and the time of arrival of the signal. In the second stage, a track extrapolated into the ASHIPH system and intersections with different parts of the counters are determined.

For the event reconstruction, the ASHIPH system needs to be aligned to the tracking system, which consists of a drift chamber and a vertex detector. The directions of the co-ordinate axes X, Y, and Z are presented in Fig. 1. For the alignment of the systems with each other, cosmic muons and Bhabha events (for the endcap) with at least one particle with a momentum of more than 1 GeV/c are used. The amplitude of the signal created by a particle that crosses the WLS is several times larger than from particles traversing the aerogel. We also know that the WLSs are each located at approximately 18° over the full azimuthal angle coverage (Fig. 4). This allows us to determine the position of each counter relative to the tracking system with 0.5–1.0 mm accuracy. This accuracy is determined by the

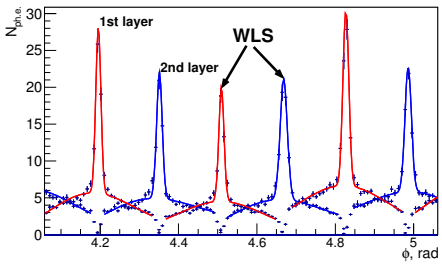

Fig. 4: Dependence of the signal amplitude of the cosmic muons (in number of photoelectrons) on the azimuthal angle φ.

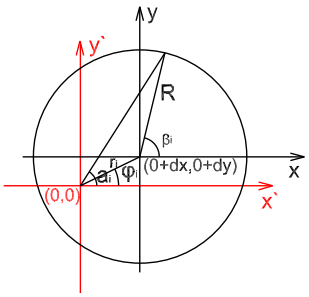

Fig. 5: Relationship between the co-ordinates of the KEDR tracking system (x', y') and the co-ordinates of the ASHIPH system (x, y).

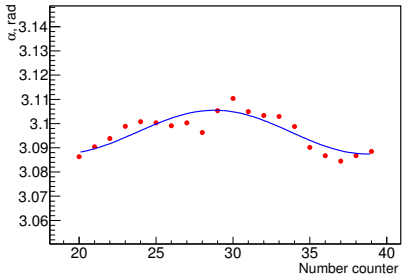

Fig. 6: Position of the WLSs in the azimuthal angle of the tracking system (x',y') normalized to the position of the WLS for one counter, together with a fit of the experimental data for determining β_i, φ_i, and r_i.

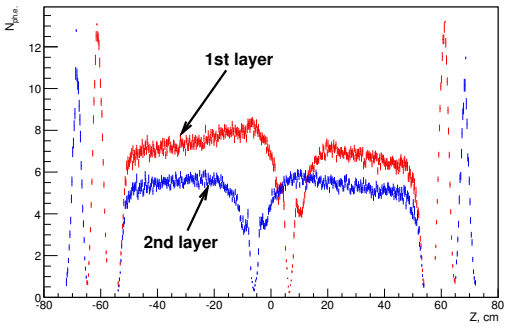

Fig. 7: Dependence of the amplitude from the cosmic muons on the Cartesian co-ordinate Z.

WLS geometry and co-ordinate resolution of the detector's drift chamber. The position of the WLS could be described by the relation between the co-ordinates of the tracking system and the geometric centre of the ASHIPH system (Fig. 5):

$$\alpha_i = \arctan\left(\frac{R\cdot\sin(\beta_i - i\cdot\pi/10) + r_i\cdot\sin(\varphi_i)}{R\cdot\cos(\beta_i - i\cdot\pi/10) + r_i\cdot\cos(\varphi_i)}\right) + (\pi/10)\cdot i\,, \qquad (1)$$

where i is number of the counter, from 0 to 159 and β_i, φ_i, r_i are parameters determined in the fit to the experimental data (Fig. 6). R is the radius of the ASHIPH system, and was measured during the installation of the system to the KEDR detector. The experimental data were fitted independently for eight geometric parts of the ASHIPH system.

The displacement along the Z co-ordinate between the ASHIPH and the tracking system was determined using the position of the midpoints of the barrel counters (Fig. 7). The rotation angle φ is determined by the displacement of the WLS relative to zero in local co-ordinates. Displacement along the angles θ and ψ of the ASHIPH system is not visible; therefore, these angles were fixed to zero. The final shifts and rotations of the ASHIPH system after alignment relative to the tracking system are presented in Table 1.

4 ASHIPH system efficiency

4.1 Geometric efficiency on Bhabha events

To measure the geometric efficiency of the system, $e^+e^- \to e^+e^-$ events called Bhabha events were selected from the experimental data using information from the tracking system (two collinear tracks

Table 1: Shifts and rotation of the ASHIPH system

	$\triangle x$, **mm**	$\triangle y$, **mm**	$\triangle z$, **mm**	$\triangle \varphi$, **rad**
Barrel	2.30 ± 0.18	-4.10 ± 0.10	2.50 ± 0.20	0.046 ± 0.001
Left endcap	1.42 ± 0.16	0.27 ± 0.06	6.00 ± 0.23	0.035 ± 0.001
Right endcap	4.28 ± 0.02	6.18 ± 0.11	0.00 ± 0.20	0.035 ± 0.001

Table 2: Geometric efficiency for the case when at least one layer is fired.

Area of counter with offset from walls	ε, %
1)'Aerogel'–0 mm	$95.7 \pm 0.6\%$
2)'Aerogel'–5 mm	$86.1 \pm 0.6\%$
3)'Aerogel'–10 mm	$76.2 \pm 0.6\%$
4)'All counter'–0 mm	$99.5 \pm 0.5\%$
5)'All counter'–5 mm	$99.1 \pm 0.6\%$
6)'All counter'–10 mm	$98.4 \pm 0.6\%$

Table 3: Geometric efficiency for the case when both layers are fired.

Area of counter with offset from walls	ε, %
1)'Aerogel'–0 mm	$84.6 \pm 0.6\%$
2)'Aerogel'–5 mm	$74.4 \pm 0.6\%$
3)'Aerogel'–10 mm	$64.5 \pm 0.5\%$
4)'All counter'–0 mm	$86.4 \pm 0.6\%$
5)'All counter'–5 mm	$76.5 \pm 0.6\%$
6)'All counter'–10 mm	$66.5 \pm 0.5\%$

from the interaction point) and the calorimeter system (total released energy tracks should be more than 2 GeV). The geometric efficiency was determined by the expression:

$$\varepsilon = \frac{N_{\text{ashiph\_tracks}}}{N_{\text{tracks}}} , \tag{2}$$

where N_{tracks} is the number of charged particle tracks and $N_{\text{ashiph\_tracks}}$ is the number of charged particle tracks that hit in the ASHIPH system. The events were selected by the calorimeter in a polar angle range covering $20^\circ < \theta < 160^\circ$ (corresponding to 94% of the full sphere surrounding the interaction point).

Two area types of the counter are considered in the following, called 'Aerogel' and 'All counter'. 'Aerogel' is the area of the aerogel with cut-offs for the electronics and WLS and offset from the walls. 'All counter' is the area of the aerogel and WLS with cut-offs for the electronics and offset from the walls. Tables 2 and 3 present the results for two different intersections of the track of the system. At least one layer fired is the case when a particle hits at least one layer of the system. Both layers fired is the case when a particle hits both layers of the system.

4.2 Efficiency of charged particle detection

The momentum dependence of the amplitude sum of the number of photoelectrons on cosmic muons for both layers in the barrel part of the system is shown in Fig. 8 [5, 8]. The data in Fig. 8 are fitted by the function:

$$\mu = \mu_0 + \mu_{\text{max}} \cdot \frac{p^2 - p_{\text{thr}}^2}{p^2} , \tag{3}$$

where p is momentum of the muon, p_{thr} is the momentum corresponding to the Cherenkov emission threshold ($p_{\text{thr}} = 322$ MeV/c for $n = 1.05$), μ_0 is the amplitude for subthreshold particles, and μ_{max} is the amplitude for relativistic particles.

The average amplitude of cosmic muons crossing the barrel counters for the first layer is 5.7 ± 0.1 photoelectrons, for the second layer, it is 4.0 ± 0.1 photoelectrons, and for the sum of both layers, it is 9.3 ± 0.4 photoelectrons. The inefficiency for a single layer is $(1 \pm 2)\%$ if the threshold is 0.1 photoelectrons while for two layers in OR mode, it is $(1 \pm 2) \cdot 10^{-2}\%$.

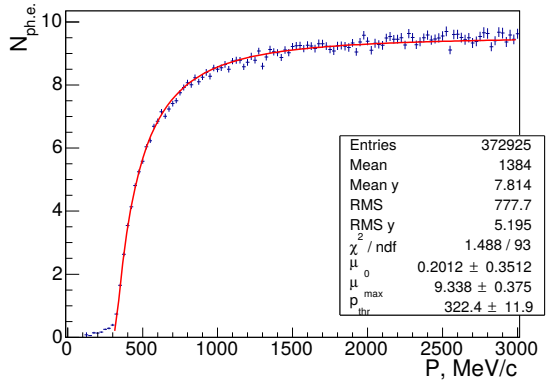

Fig. 8: The amplitude dependence of the barrel counters on the momentum of the cosmic muons which crossed two layers of aerogel in the KEDR ASHIPH system.

4.3 Investigation of detection efficiency

To evaluate the kaon identification efficiency and pion misidentification, a data set with muons of corresponding momentum were chosen from cosmic muons [5]. Muons with a momentum from 200 to 300 MeV/c were chosen as the under-threshold particles. They have the same velocities as kaons with a momentum range of $940 < P_{\mathrm{K}} < 1430$ MeV/c. Muons with a momentum range of 700 to 1100 MeV/c were chosen as the relativistic particles. They correspond to pions with the same momentum, $940 < P_{\pi} < 1430$ MeV/c. Several approaches for particle registration with two layers of the system were investigated:

– 'AND'—a relativistic particle gives a signal in both layers of the system;
– 'OR'—a relativistic particle gives a signal in at least one layer of the system;
– 'THICK'—the sum of the amplitudes in both layers exceeds the threshold.

For the approaches 'THICK', 'OR', and 'AND', the momentum dependencies of kaon registration efficiency and pion misidentification are presented in Fig. 9. For the 'THICK' option, the threshold is equal to 2.0 photoelectrons; for the two other approaches, the threshold is equal to 0.5 photoelectrons. The working momentum region is shown by vertical dashed lines. From these data it is possible to determine the separation power in terms of σ:

$$K[\sigma] = \mathrm{erf}^{-1}(-1 + 2\varepsilon_{\mathrm{K}}) + \mathrm{erf}^{-1}(-1 + 2\varepsilon_{\pi}) \,, \tag{4}$$

where ε_{K} is the identification efficiency for kaons and ε_{π} is the identification efficiency for pions. In the momentum range 0.95–1.45 GeV/c, π/K separation of better than 4σ can be extracted.

5 Simulation of ASHIPH counters

The simulation is performed using a Monte Carlo code based on the Geant3.21 package. The Geant3.21 description of the ASHIPH counters is integrated into the KEDR full detector simulation, which is used for KEDR performance studies and the production of simulated event data, needed for the data analysis. The simulation of the ASHIPH system includes a realistic geometric description of all 160 counters (three active media—aerogel, shifter, Teflon; electronics boxes; and HV outputs). For all counters, a realistic aerogel refractive index was used and measured inhomogeneities in the light collection are taken into account. The digitized amplitudes from calibrated single-photon spectra and pulse shapes are generated.

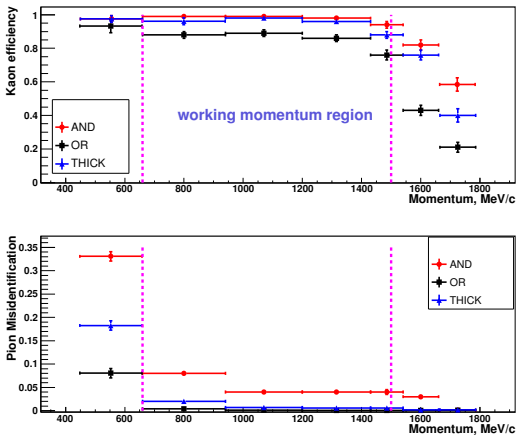

Fig. 9: Momentum dependence of kaon identification efficiency and pion misidentification (obtained from cosmic muons with corresponding velocity).

The full signal from a particle in the ASHIPH counter is the sum of the Cherenkov signal and the scintillation signal in aerogel, shifter, and Teflon:

$$I = I_{\text{ch\_aer}} + I_{\text{ch\_sh}} + I_{\text{ch\_tef}} + I_{\text{sc\_aer}} + I_{\text{sc\_sh}} + I_{\text{sc\_tef}} \, . \tag{5}$$

The magnitude of scintillation is proportional to the energy loss in matter:

$$I_{\text{sc}_i} = \alpha_i \Delta E_i \, , \tag{6}$$

where α_i is the proportionality factor and i is the index of the geometric volume (aerogel, shifter, or Teflon).

The number of Cherenkov photoelectrons from relativistic particles above the threshold is determined as:

$$I_{\text{ch}_i} = \frac{\mathrm{d}N_i}{\mathrm{d}x_i} = K_i \cdot z^2 (1 - \frac{1}{(n_i \beta)^2}) \, , \tag{7}$$

where n_i is the refraction index and K_i is the proportionality factor, taking into account the inhomogeneity of light collection, $\beta = \upsilon / c$.

The proportionality factor from experimental data is determined as:

$$K_i = \frac{\frac{N_{\text{ph.e.}}}{L_{\text{track}}}}{z^2 \left(1 - \frac{1}{(n_i \beta)^2}\right)} \, , \tag{8}$$

where $N_{\text{ph.e.}}$ is the number of photoelectrons and L_{track} is the track length in counter. To account for the inhomogeneity of the light collection in the counter, partition of aerogel and WLS was done for five different types of counter. The proportionality factor for each area was determined using cosmic muons with momentum more than 1 GeV/c (Figs. 10 and 11) and used in the simulation program. The results of the inhomogeneity of the light collection are presented in Table 4.

The amplitude distribution of the number of photoelectrons is not described by the Poisson distribution, owing to fluctuations in the gain. To generate a real amplitude, the function distribution is used, which is obtained by a convolution of single-electron spectrum with a Poisson distribution:

$$F(x) = \sum_{n=0}^{n=25} P_n f_n(x) \, , \tag{9}$$

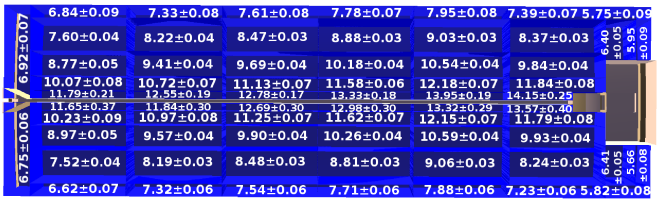

Fig. 10: Distribution of proportionality factor averaged over all long barrel counters of the first layer.

Fig. 11: Distribution of the proportionality factor averaged over all endcap counters.

Table 4: Inhomogeneity of light collection (relative error) for five types of counter

Type of counter	Inhomogeneity of light collection
Short counter of first layer	±26%
Long counter of first layer	±25%
Short counter of second layer	±32%
Long counter of second layer	±36%
Endcap counter	±19%

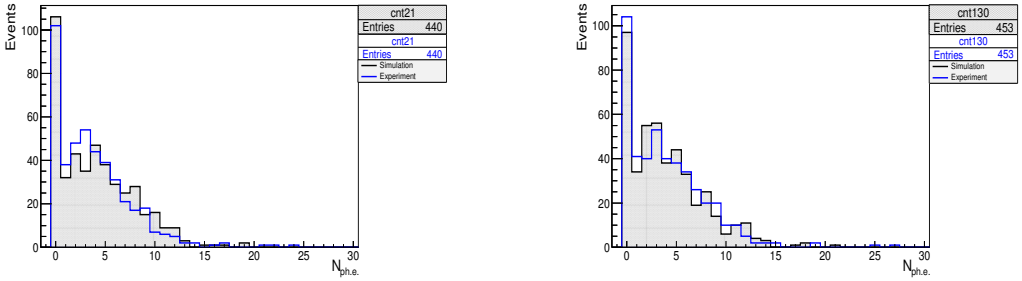

Fig. 12: Distribution of the number of photoelectrons from cosmic muons in simulation and data

where $f_n(x)$ is given by

$$f_n(x) = \int f_1(y) f_{n-1}(x-y)\mathrm{d}y \,, \tag{10}$$

P_n is the Poisson distribution, and $f_1(x)$ is the single-photoelectron spectrum.

Figure 12 presents a comparison of the distribution of the number of photoelectrons from cosmic muons obtained in simulation with experimental data. The comparison of histograms was achieved using the χ^2 criterion. For example, the 21 counter has $\chi^2/\mathrm{ndf} = 1.06$ and the 130 counter has $\chi^2/\mathrm{ndf} = 0.99$. The integral of the efficiency for these amplitude spectra is presented in Fig. 13. The detection efficiency at a threshold of 0.5 photoelectrons is greater than 98%.

6 Summary

The ASHIPH technique of Cherenkov light collection was developed at BINP. It allowed us to decrease significantly the necessary photocathode area and production costs. An event reconstruction program for the ASHIPH system was developed. Alignment of the ASHIPH counters was performed. The average number of photoelectrons for relativistic cosmic muons (> 1 GeV/c) that cross both counter layers is 9.3 ± 0.4. The detection efficiency for muons with ($700 < p_\mu < 1100$ MeV/c) is 99.3±0.1% for a threshold at an amplitude sum equal to 2.0 photoelectrons. The detection efficiency for under-threshold muons ($200 < p_\mu < 300$ MeV/c) using the same approach is $3 \pm 1\%$. These data correspond to a π/K

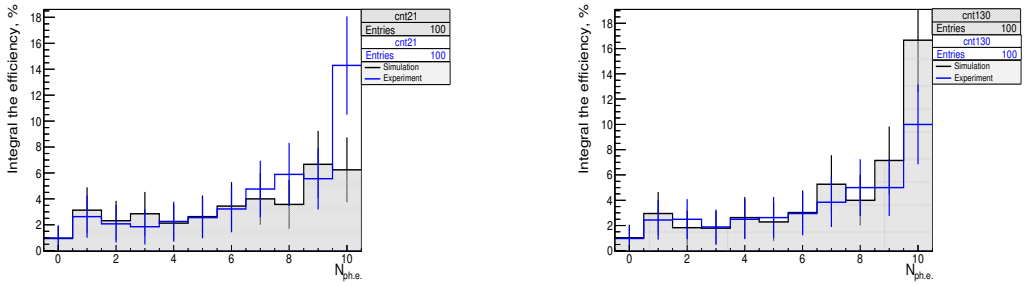

Fig. 13: Integral of the efficiency for amplitude spectra from simulation and data

separation better than 4σ in the momentum range 0.95–1.45 GeV/c. The geometric efficiency for Bhabha events was measured. In the case when a particle hits at least one layer of the system, the geometric efficiency is 96%. The inhomogeneity of the light collection of the ASHIPH counters with cosmic muons was measured. The inhomogeneity of light collection for barrel and endcap counters is $\pm$30% and $\pm$19% respectively. A simulation program for the ASHIPH counters was developed.

References

[1] A. Onuchin *et al.*, *Nucl. Instrum. Methods* **A315** (1992) 517. https://doi.org/10.1016/0168-9002(92)90757-U

[2] M.Y. Barnykov *et al.*, *Nucl. Instrum. Methods* **A419** (1998) 584. https://doi.org/10.1016/S0168-9002(98)00871-7

[3] A.Y. Barnyakov *et al.*, *Nucl. Instrum. Methods* **A494** (2002) 424. https://doi.org/10.1016/S0168-9002(02)01513-9

[4] A.Y. Barnyakov *et al.*, *Nucl. Instrum. Methods* **A478** (2002) 353. https://doi.org/10.1016/S0168-9002(01)01828-9

[5] A.Y Barnyakov *et al.*, *Nucl. Instrum. Methods* **A824** (2016) 79. https://doi.org/10.1016/j.nima.2015.10.105

[6] V.M. Aulchenko e*t al.*, *Nucl. Instrum. Methods* **A409** (1998) 639. https://doi.org/10.1016/S0168-9002(98)00088-6

[7] V.V. Anashin *et al.* (KEDR collaboration), *Phys. Part. Nucl.* **44** (2013) 657. https://doi.org/10.1134/S1063779613040035

[8] A.Y. Barnyakov *et al.*, *J. Instrum.* **9** (2014) C08010. https://doi.org/10.1088/1748-0221/9/09/C09005